Original scientific paper
https://doi.org/10.33180/InfMIDEM2022.104

Informacije MIDEM
Journal of Microelectronics,
Electronic Components and Materials
Vol. 52, No. 1(2022), 29 – 39

Throughput Estimation of K-zone Gbps Radio Links Operating in the E-band

Attila Hilt[1,2]

[1]Nokia Cloud and Network Services, Budapest, Hungary
[2]Department of Broadband Infocommunications and Electromagnetic Theory, Faculty of Electrical Engineering and Informatics, BME, Budapest University of Technology and Economics, Budapest, Hungary

Abstract: Nowadays covid virus changes our work, learning and life-style. Broadband telecommunication channels are required for remote work, e-learning and video conferencing. Optical-fiber access offers the required wide bandwidths and low latencies. However, due to technical and business reasons optical-fiber cannot yet reach all homes, all offices or industrial plants. Mobile network sites often meet similar problems in urban environment. Since the introduction of mobile data (e.g., High-Speed Packet Access in 3G networks) and with the actual 4G expansion and 5G deployments, more and more cell-sites are connected to the fiber backhaul. But not all radio nodes can benefit the enormous bandwidth provided by optical-fiber access. The missing section between the fiber end-point and the site is often only few hundred meters, one or two kilometers. More and more millimeter-wave radios are deployed to reach the fiber access point. As radio links suffer from rain, atmospheric attenuation and interference, careful design is required. This paper focuses on digital radio links operating in the *E*-band (71-86 GHz) in Central Europe, where rainfall rates reach 42 mm/h (e.g., Slovenia and Hungary). In the paper a step-by-step planning method is shown to estimate the yearly radio throughput. It is shown that E-band radio links can reach Gigabit/s (Gbps) speed and availability figures comparable to optical-fiber connections.

Keywords: fiber/wireless system; millimeter-wave; *E*-band; Gbps radio access; adaptive modulation; throughput; rainfall

Ocena zmogljivosti gigabitne radijske zveze v območju K v pasu E

Izvleček: Danes virus covid spreminja naše delo, učenje in življenjski slog. Za delo na daljavo, e-učenje in videokonference so potrebni širokopasovni telekomunikacijski kanali. Dostop z optičnimi vlakni ponuja zahtevane široke pasovne širine in nizke zakasnitve. Vendar zaradi tehničnih in poslovnih razlogov optična vlakna še ne morejo doseči vseh domov, pisarn ali industrijskih obratov. Mobilna omrežna mesta se v mestnem okolju pogosto srečujejo s podobnimi težavami. Od uvedbe mobilnih podatkov (npr. hitri paketni dostop v omrežjih 3G) ter z dejanskim širjenjem omrežja 4G in uvajanjem omrežja 5G je vse več lokacij priključenih na optično hrbtno povezavo. Vendar pa vsa radijska vozlišča ne morejo izkoristiti ogromne pasovne širine, ki jo zagotavlja dostop z optičnimi vlakni. Manjkajoči odsek med končno točko optičnega omrežja in lokacijo je pogosto le nekaj sto metrov, en ali dva kilometra. Razvitih je ved več radijskih sprejemnikov z milimetrskimi valovi, da bi dosegli dostopno točko z optičnimi vlakni. Ker so radijske povezave izpostavljene dežju, atmosferskemu slabljenju in motnjam, je potrebno skrbno načrtovanje. Članek se osredotoča na digitalne radijske povezave, ki delujejo v pasu *E* (71-86 GHz) v Srednji Evropi, kjer količina padavin doseže 42 mm/h (npr. v Sloveniji in na Madžarskem). V članku je prikazana metoda načrtovanja po korakih za oceno letne radijske prepustnosti. Pokazano je, da lahko radijske povezave v pasu E dosežejo hitrosti gigabit/s (Gb/s) in razpoložljivost, primerljivo s povezavami z optičnimi vlakni.

Ključne besede: optični/brezžični sistem; milimetrski valovi; gigabitni radijski dostop; *E* pas; prilagodljiva modulacija; prepustnost; stopnja padavin

** Corresponding Author's e-mail: attila.hilt@nokia.com, hilt.attila@vik.bme.hu*

How to cite:
A. Hilt, "Throughput Estimation of K-zone Gbps Radio Links Operating in the E-band", Inf. Midem-J. Microelectron. Electron. Compon. Mater., Vol. 52, No. 1(2022), pp. 29–39

1 Introduction

There is an intensive ongoing research of combined fiber-optical/wireless networks [1]-[6]. Remarkably, the investigations of using microwave and millimeter-wave (μW/mmW) frequencies in combined fiber/wireless networks started more than two decades ago [7]-[11]. In both fixed and mobile access systems, the optical fibers are deployed to reach the end-users as close as possible. The actual covid virus changed our workstyle. Remote work, e-learning and videoconferencing require broadband access. Fiber access systems, such as FTTH (Fiber-to-the-Home, Fig. 1.a) and FTTO (Fiber-to-the-Office, Fig. 1.b) became even more important during pandemic times [12]. The optical fiber can provide the required bandwidth for the users. The wireless part e.g., WiFi can provide some mobility in FTTH or FTTO access systems, when needed.

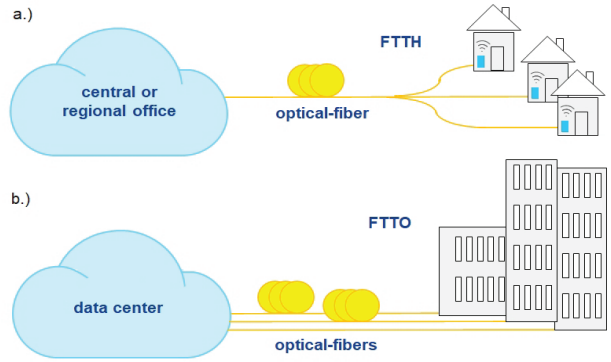

Figure 1: a.) Fiber-to-the-Home and b.) Fiber-to-the-Office systems.

In 2G (2nd generation) and early 3G (3rd generation) mobile systems fiber-optical technology was mainly used in the core and transport parts of the network [13]-[14]. With the introduction of HSPA (High Speed Packet Access) and LTE (Long Term Evolution) broadband for mobile data became a reality. FTTS (Fiber-to-the-Site) turned out to be more and more important. As shown in Fig. 2, new and newer Radio Access Technologies (RATs) like 4G, 5G employ FTTS wherever it is possible.

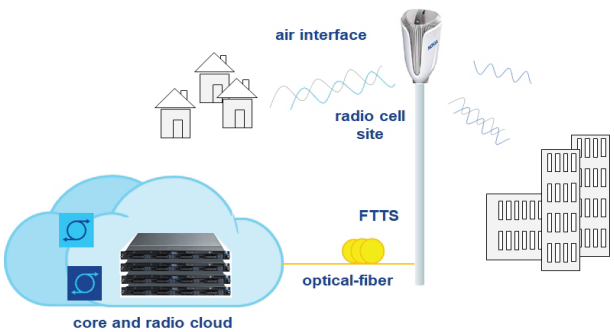

Figure 2: Fiber-to-the-Site.

Beside the enormous bandwidth, optical fibers can provide the low latency that are essential requirements in 5G and future 6G mobile systems [15]-[16]. The wireless μW/mmW access part offers mobility for the end users.

Unfortunately, the initial deployment of optical fibers is a slow and expensive process. Especially in urban environment, the installation of optical cables may require heavy construction works (i.e., cable tunnels) resulting in temporary closure of pavements and street sections. Thus, optical fibers cannot yet reach all the radio cell sites. In several cases a few hundred meters gap remains between the optical-fiber end-point or 'aggregation point' and the cell-site or end user. In such scenarios, *E*-band millimeter-wave fixed radio links can connect the last few-hundred meters where optical fiber is not yet laid down (Fig. 3). It is important to mention, that these Gigabit/s radio connections can be re-used later on at other sites, when optical fiber finally arrives. In practice, the very dense fixed radio and optical network is continuously evolving in big cities (Fig. 3). The radio links are getting shorter and shorter, but higher and higher transmission capacities are expected.

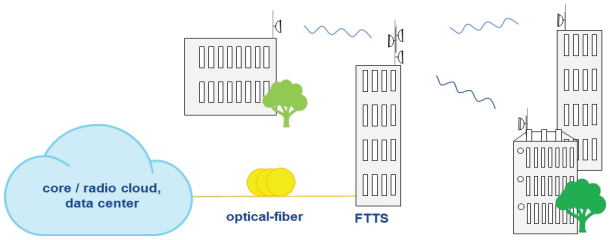

Figure 3: Fiber-radio access node.

This paper reviews the main characteristics of the *E*-band radios and summarizes the planning steps of these links. As shown, clearance and rainfall are the main factors determining link availability. Finally, calculation results are shown for *K* rain-zone that covers Central Europe, including Slovenia and Hungary. In the given design example, average link throughput is estimated. It is shown that state-of-the-art *E*-band radios can bring 'fiber-availability' with proper radio link design.

2 Line-of-Sight E-band radio links

μW/mmW radio links offer a good solution to connect the fiber-end-point with the nearby site or office. An important design rule is that the radio links require clean Line-of-Sight (LoS). Obstacles, especially metal objects may cause unwanted reflections. When the direct radio wave and the reflected wave arrive to the

receiving antenna with opposite phase, the two signals cancel each other. Even though the exact cancellation happens at one (or multiple) discrete frequency, the attenuation due to non-satisfactory clearance can be significant for wide bandwidth (BW) radio signals too. In practice the LoS condition is estimated with the clearance of the first Fresnel-zone. The radius of the *n*-th Fresnel-ellipsoid is calculated as [17], [18]:

$$F_n\left[\mathrm{m}\right]=\sqrt{n\cdot\frac{d_1\cdot d_2}{d_1+d_2}\cdot\lambda}=\sqrt{c\cdot n\cdot\frac{d_1\cdot d_2}{f\cdot d}} \quad (1)$$

Where $d=d_1+d_2$ is the total hop length of the link, f is the frequency and $c\approx 299.7\cdot 10^8$ m/s is the speed of light in free space. As shown in Fig. 4, d_1 and d_2 are the distances measured from the axial observation point to antenna 1 and antenna 2, respectively. To avoid doubts, in the coming equations units are indicated in brackets. Eq. (1) simplifies for the first Fresnel-zone with n=1. When d is given in km and f is given in GHz, then:

$$F_1\left[\mathrm{m}\right]=17.312\sqrt{\frac{d_1\cdot d_2}{f\cdot d}} \quad (2)$$

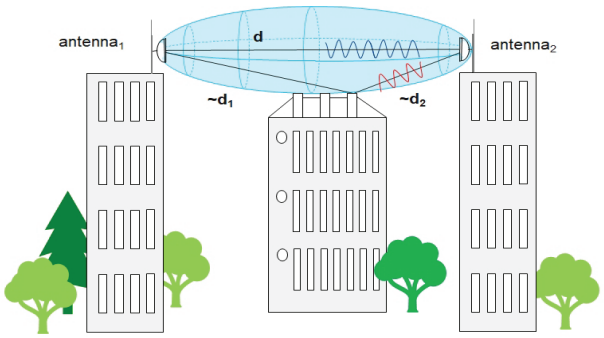

Figure 4: Unwanted reflection from an obstacle in the first Fresnel-zone.

Please note, that equation (2) has different forms when frequency and distance are given in other units [17], [18]. Let us consider an *E*-band radio, operating at f=71.125 GHz with a hop length of d = 1.2 km. The maximum radius of the first Fresnel-ellipsoid is at the middle of the link where $d_1=d_2=d/2$:

$$F_1\left[\mathrm{m}\right]\cong 17.312\sqrt{\frac{d}{2}\cdot\frac{d}{2}\cdot\frac{1}{f\cdot d}}=8.656\sqrt{\frac{d\left[\mathrm{km}\right]}{f\left[\mathrm{GHz}\right]}}\cong 1.1\left[\mathrm{m}\right], \quad (3)$$

In practice, a narrow ø 2.2 m diameter ellipsoid shall be clean between the two transceivers of the radio link. As an initial check, the LoS condition is usually investigated first in a radio link planning tool. An example path profile is shown in Fig. 5, as it is seen in IQ-Link tool [19]. For the proper design accurate coordinates are necessary. A useful help if a high-resolution digital terrain model is added to the link planning tool. Clutter info and three-dimensional (3D) building data can make the preliminary LoS check more reliable.

Figure 5: Path profile of the mmW radio link, as seen in the IQ-link planning tool [19].

An attractive LoS estimation is possible by visualizing the planned link in Google-Earth three dimensional plot. Figure 6 shows the d=1.2 km long link designed in an inner district of Budapest. Please note, that computer estimations are never accurate enough in urban environments. Buildings, chimneys, trees, cables or cranes may attenuate or block completely the *E*-band link. Site visits are necessary to confirm LoS before constructing the *E*-band link. In the rest of this paper a clear LoS condition is assumed.

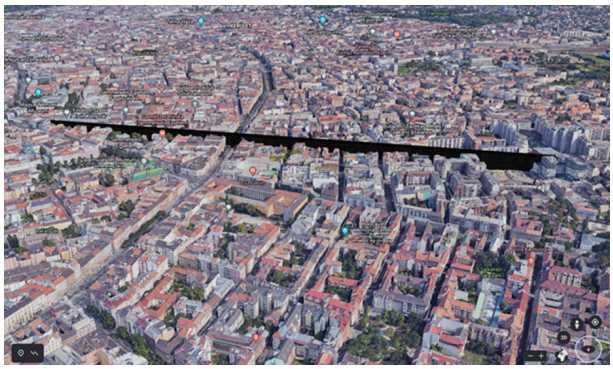

Figure 6: Line-of-Sight estimation using Google Earth in the microwave link design.

3 Radios with adaptive modulation

For calculation simplicity, in the paper a single *E*-band radio connection is investigated. To calculate aggregat-

ed throughput of dual frequency or dual polarization radio links (e.g., 23 GHz and *E*-band radios combined onto one dual-band antenna) is not discussed. But the presented design method can be extended to include the lower frequency band or the other polarization too.

The main characteristics of the *E*-band millimeter-wave digital radios are demonstrated in the following by selecting the Nokia 'Wavence' radio. Wavence radio family uses adaptive modulation [20]. It is emphasized that the presented design method is general, and applicable for any other state-of the-art *E*-band digital radio having adaptive modulation [17]-[22]. In case of fading, adaptive modulation radios automatically switch to simpler modulation mode. Simpler modulation modes are less sensitive to attenuation. Thus, the radio connection is not lost. The transmission is maintained, even though the radio throughput is reduced to a lower bit rate [17]-[22].

For simplicity, in Table 1, the radio parameters are given only for the 250 MHz, 500 MHz, 1 GHz and 2 GHz radio frequency (RF) bandwidth (BW) settings. As seen, the modulation mode can vary from 512-QAM (Quadrature Amplitude Modulation) to QPSK (Quadrature Phase Shift Keying) and BPSK (Binary Phase Shift Keying). The Wavence radio RF bandwidth can be set to 62.5 MHz, 125 MHz, 250 MHz, 500 MHz, 750 MHz, 1 GHz, 1.25 GHz, 1.5 GHz or 2 GHz. The values listed in Table 1 are typical equipment values specified for the Bit Error Rate of $BER=10^{-6}$. System Gain (SG, in decibel) is defined as the difference of the transmit (Tx) power and the receiver (Rx) threshold level:

$$SG_{\text{mod}-n}\left[\text{dB}\right] = P_{\text{Tx}}\left[\text{dBm}\right] - P_{\text{Rxth}}\left[\text{dBm}\right]. \quad (4)$$

Table 1: Tipical *E*-band radio parameters

BW	250 MHz	500 MHz	1 GHz	2 GHz
Modulation	System Gain [dB] at BER=10^{-6}			
BPSK 1/4		94.7	91.4	86
BPSK 1/2	94.9	91.7	88.4	83
BPSK	91.9	88.7	85.4	80
QPSK	88.9	85.7	82.4	77
16-QAM	80.3	77.2	73.8	67.9
32-QAM	77.2	74.1	70.7	64.7
64-QAM	74.3	71.1	67.6	58
128-QAM	71.2	66.9	63.3	54.3
256-QAM	66	62.7	58	
512-QAM	61	57.5		

In Eq. (4) mod-*n* refers to the actual modulation mode that is adaptively varying between BPSK 1/4 and 512-QAM, according to propagation conditions. In practice, we have as many System Gain figures as many modulation modes are available in the selected channel BW. BPSK 1/2 denotes a BPSK modulation where the RF channel is halved. When the same signal power remains with half of the noise in the receiver, the SG is increased with 3 dB. Similarly, BPSK 1/4 reduces the BW to its quarter, so SG is 6 dB better than that of BPSK. (It is important to specify *BER* properly when SG and Fading Margin (FM) figures are given. Please note, that Rx thresholds for $BER=10^{-3}$ are lower than for $BER=10^{-6}$. As SG values at $BER=10^{-3}$ are higher, it is important to check, which figures are used to avoid planning mistake.) In Eq. (4), antenna gain is not added into the definition of SG. Note, that other definition exists too [22].

4 Link design and rain attenuation

Having the System Gain values for the different modulation modes in the selected RF bandwidth, it is possible to calculate the Fading Margin of the link. In this part we discuss the main fading factors. It is shown that rainfall has the most severe effect on the transmission quality. As shown, FM can be consumed by atmospheric and rain attenuation. During sunny days high FM is not required. Automatic Transmit Power Control (ATPC) can reduce output power to avoid unwanted interference in other links and to save energy. Threshold degradation due to radio-interference from other links is not discussed here. It is an assumption that radio channel is properly selected.

4.1 Fading margin calculation

The radio-link operates with a given modulation mode, as long as its Fading Margin is higher than the sum of all kind of different link losses:

$$FM_{\text{mod}-n}^{[\text{dB}]} > A_{\text{rain}}^{[\text{dB}]} + A_{\text{atm}}^{[\text{dB}]} + A_{\text{obst}}^{[\text{dB}]}. \quad (5)$$

In our design a clean LoS condition is considered, so there is no obstacle loss, A_{obst} is zero. FM remains for the main propagation factors of rain attenuation (A_{rain}) and atmospheric attenuation (A_{atm}). Without losing validity of the statements, in the following *B*W = 1 GHz bandwidth is selected in the calculation examples. In Eq. (5) mod-*n* again refers to the actual modulation mode. It can vary between BPSK 1/4, BPSK 1/2, BPSK, QPSK, 16-QAM, 64-QAM, 128-QAM and 256-QAM. For 1 GHz BW the corresponding Ethernet throughput figures are 200, 400, 800 Mbps, 1.6, 3.2, 4, 5.6 and 6.4 Gbps, respectively. If link losses consume the fade margin, the link automatically changes its modulation mode to a less sensitive one. Fading Margin is calculated as [22]:

$$FM^{[\mathrm{dB}]} = P_{\mathrm{Tx}}^{[\mathrm{dBm}]} + G_{\mathrm{Tx}}^{[\mathrm{dBi}]} + G_{\mathrm{Rx}}^{[\mathrm{dBi}]} - FSL^{[\mathrm{dB}]} - P_{\mathrm{Rxth}}^{[\mathrm{dBm}]}, \quad (6)$$

where G_{TX} and G_{RX} are the transmit and receive antenna gain values and *FSL* denotes the Free Space Loss:

$$FSL^{[\mathrm{dB}]} = 92.44 + 20log_{10}\left(f^{[\mathrm{GHz}]}\right) + 20log_{10}\left(d^{[\mathrm{km}]}\right). \quad (7)$$

Combining equations (4) and (6):

$$FM_{\mathrm{mod}-n}^{[\mathrm{dB}]} = SG_{\mathrm{mod}-n}^{[\mathrm{dB}]} + G_{\mathrm{Tx}}^{[\mathrm{dBi}]} + G_{\mathrm{Rx}}^{[\mathrm{dBi}]} - FSL^{[\mathrm{dB}]}. \quad (8)$$

It is visible in Eq. (8), that for a given frequency (*E*-band), and given link distance, only a few parameters remain free: BW, antenna size and modulation mode. Nokia Wavence radios can have ø 12 cm integrated antennas or slip mount antennas. Table 2 below summarizes the possible Tx and Rx antenna combinations and their overall Gain. The 1 foot and 2 feet antennas are calculated with their mid-band gain, as specified in [23]-[24].

Increasing the fade margin by proper link design, the rain attenuation can be compensated and thus the throughput of the digital link can be maximized. The following calculations are performed with different single-polarization antenna sizes according to Table 2.

Table 2: Antenna pairs and their Gain

antenna diameters ø [cm]	Antenna Gain and type			
	G_{Tx} [dBi]	G_{Rx} [dBi]	$G_{Tx} + G_{Rx}$ [dB]	single, linear polarization
12 – 12	38	38	76	integrated
12 – 38	38	43.5	81.5	int. + VHLP1
38 – 38	43.5	43.5	87	VHLP1 [23]
38 – 66	43.5	50.5	94	VHLP1+VHLP2
66 – 66	50.5	50.5	101	VHLP2 [24]

4.2 Calculation of atmospheric attenuation

Atmospheric attenuation is caused by the absorption of gaseous particles in the air [25]. Water vapor causes extra attenuation of 0.2 dB/km around 23 GHz and 12 dB/km around 180 GHz. High attenuation peaks are caused by oxygen absorption in the 56–64 GHz (16 dB/km) and in the 120 GHz (2 dB/km) range [25]-[27].

Compared to rain attenuation, atmospheric attenuation is negligible for short links at the 71-86 GHz communication frequencies of *E*-band. In the calculations, specific attenuation of γ_{atm}=0.4 dB/km is used [25]. The total atmospheric attenuation is calculated for the entire link length using the specific attenuation:

$$A_{\mathrm{atm}}\left[\mathrm{dB}\right] = \gamma_{\mathrm{atm}}\left[\mathrm{dB/km}\right] \cdot d\left[\mathrm{km}\right] \quad (9)$$

The entire atmospheric attenuation for a *d*=1.2 km long link is less than 0.5 dB. For practical calculation reasons, the Fade Margin discussed in part 4.1 is decreased with this linear atmospheric attenuation value. A new fade margin figure can be introduced, a FM that remains only for the rain fading for clean LoS paths:

$$FM_{\mathrm{mod}-n}^{[dB]} - A_{\mathrm{atm}}^{[\mathrm{dB}]} > A_{\mathrm{rain}}^{[\mathrm{dB}]}. \quad (10)$$

Equation (10) is similar to Eq. (5), but this form is more useful for numerical calculations. As it is shown in the next part, rain attenuation calculation leads to an equation that is difficult to solve mathematically. However, with a simple program it is easy to calculate the results numerically.

4.3 Calculation of rain attenuation for K-zone

According to ITU-R (Radiocommunication Sector of the International Telecommunication Union), the attenuation of radio waves due to rainfall can be estimated as:

$$\gamma_{\mathrm{rain}}\left[\mathrm{dB/km}\right] = kR^{\alpha} \quad (11)$$

where *R* is the rainfall-rate, given in mm/h [28]. Constants *k* and α depend on the frequency and polarization (either vertical or horizontal) of the link [28]. γ_{rain} is the specific attenuation of rain in dB/km units. When constants *k* and α are plotted as a function of frequency, it is visible that the horizontal and vertical values are very similar in the 71-86 GHz band (shadowed with blue in Fig. 7). Unlike in the traditional 18-38 GHz communication bands (shadowed with grey in Fig. 7), the polarization of the radio link has seemingly less impact on rain attenuation in the *E*-band. This can be explained by stormy winds that are usually accompanying intensive rainfalls, thus modifying the vertical direction of rain, and by the short wavelengths of λ = 4.2…3.5 mm. Naturally, the model is to be verified with real radio measurements, that are possible with state-of the-art *E*-band radios. For this purpose, long

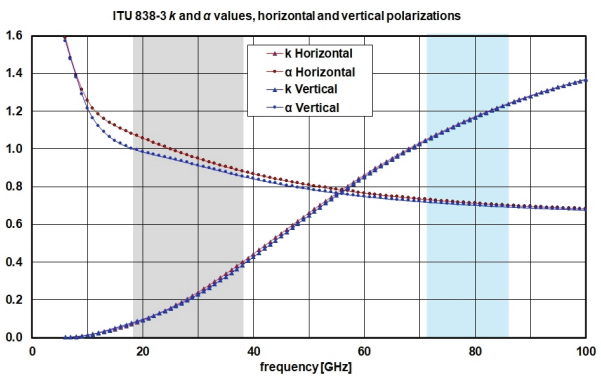

Figure 7: *k* and α parameters according to ITU [28]

BW		71 125															73 125
125	R	R1 / R'1	R2 / R'2	R3 / R'3	R4 / R'4	R5 / R'5	R6 / R'6	R7 / R'7	R8 / R'8	R9 / R'9	R10 / R'10	R11 / R'11	R12 / R'12	R13 / R'13	R14 / R'14	R15 / R'15	R16 / R'16
MHz	low fr.	71 187.5	71 312.5	71 437.5	71 562.5	71 687.5	71 812.5	71 937.5	70 062.5	72 187.5	72 312.5	72 437.5	72 562.5	72 687.5	72 812.5	72 937.5	73 062.5
raster	high fr.	81 187.5	81 312.5	81 437.5	81 562.5	81 687.5	81 812.5	81 937.5	80 062.5	82 187.5	82 312.5	82 437.5	82 562.5	82 687.5	82 812.5	82 937.5	83 062.5
250	P	P1 / P'1		P2 / P'2		P3 / P'3		P4 P'4		P5 / P'5		P6 / P'6		P7 / P'7		P8 / P'8	
MHz	low fr.	71 250		71 500		71 750		72 000		72 250		72 500		72 750		73 000	
raster	high fr.	81 250		81 500		81 750		82 000		82 250		82 500		82 750		83 000	
500	S	S1 / S'1				S2 / S'2				S3 / S'3				S4 / S'4			
MHz	low fr.	71 375				71 875				72 375				72 875			
raster	high fr.	81 375				81 875				82 375				82 875			
1	T	T1 / T'1								T2 / T'2							
GHz	low fr.	71 625								72 625							
raster	high fr.	81 625								82 625							
2	U	U1 / U'1															
GHz	low fr.	72 125															
raster	high fr.	82 125															
		81 125															83 125

BW		73 625															75 625
125	R	R21/R'21	R22/R'22	R23/R'23	R24/R'24	R25/R'25	R26/R'26	R27/R'27	R28/R'28	R29/R'29	R30/R'30	R31/R'31	R32/R'32	R33/R'33	R34/R'34	R35/R'35	R36/R'36
MHz	low fr.	73 687.5	73 812.5	73 937.5	74 062.5	74 187.5	74 312.5	74 437.5	74 562.5	74 687.5	74 812.5	74 937.5	75 062.5	75 187.5	75 312.5	75 437.5	75 562.5
raster	high fr.	83 687.5	83 812.5	83 937.5	84 062.5	84 187.5	84 312.5	84 437.5	84 562.5	84 687.5	84 812.5	84 937.5	85 062.5	85 187.5	85 312.5	85 437.5	85 562.5
250	P	P11 / P'11		P12 / P'12		P13 / P'13		P14 / P'14		P15 / P'15		P16 / P'16		P17 / P'17		P18 / P'18	
MHz	low fr.	73 750		74 000		74 250		74 500		74 750		75 000		75 250		75 500	
raster	high fr.	83 750		84 000		84 250		84 500		84 750		85 000		85 250		85 500	
500	S	S6 / S'6				S7 / S'7				S8 / S'8				S9 / S'9			
MHz	low fr.	73 875				74 375				74 875				75 375			
raster	high fr.	83 875				84 375				84 875				85 375			
1	T	T3 / T'3								T4 / T'4							
GHz	low fr.	74 125								75 125							
raster	high fr.	84 125								85 125							
2	U	U2 / U'2															
GHz	low fr.	74 625															
raster	high fr.	84 625															
		83 625	note: 750 MHz raster is not shown														85 625

Figure 8: A section of the E-band frequency allocation table with different RF bandwidths (BW).

term measurements are running in experimental links [26],[27],[29],[30].

The rain attenuation can be estimated following ITU-R P.530 [31]:

$$A_{0.01\%}\left[\mathrm{dB}\right] = \gamma_{\mathrm{rain}} \frac{d}{1 + d / 35 \cdot e^{-0.015 \cdot R_{0.01\%}}} \qquad (12)$$

$A_{0.01\%}$ means rain attenuation, that is exceeded in 0.01% of the time. Please note that Eq. (12) is recommended up to maximum R=100 mm/h rainfall rates. Central European countries falling into *K* rain-zone satisfy this constraint with the value of $R_{0.01\%}$ = 42 mm/h [22], [32]. Finally, combining Equations (10), (11) and (12) we get:

$$FM_{\mathrm{mod}-n}^{[dB]} - A_{\mathrm{atm}}^{[\mathrm{dB}]} > k \cdot R_{0.01\%}^{\alpha} \frac{d}{1 + d / 35 \cdot e^{-0.015 \cdot R_{0.01\%}}}. \qquad (13)$$

Equation (13) raises some difficulties. First, it gives estimation only for the 0.01% of time, when the rainfall is 42 mm/h or more intensive. This means, that we can split the radio modulation modes into two groups only. One group that can survive the rain in 0.01% of the time and another group that cannot tolerate this rainfall intensity. For rain probabilities in the range of p=0.001% to p=1% in time, ITU-R P.530-13 recommends the estimation for latitudes of 30° or higher [31]:

$$A_p\left[\mathrm{dB}\right] = 0.12 \cdot A_{0.01\%}\left[\mathrm{dB}\right] \cdot p^{-(0.546 + 0.043 \cdot log_{10} p)}. \qquad (14)$$

Using Eq. (14), 0.01 % can be extended into the 0.001 % - 1 % range of time, where link availabilities correspond to 99 % - 99.999 %, respectively.

The other difficulty is to find exact mathematical solution of Eq. (13), (14). Here a simple program is used for numerical solution. In a *for* cycle, the hop length can be increased in very small steps (e.g., 10 m) to find the link distance where rain attenuation consumes the fade margin of the link for the modulation mode set. The results are detailed in part 5.

4.4 Local rainfall rate statistics in K-zone

Figure 9 shows rainfall-rates measured by OMSZ, the Hungarian Meteorological Service over two decades in Budapest [33]. OMSZ operates seven meteorological stations in the capital. Fig. 9 shows rain intensities at "Belterület" station where the highest mm/h rainfall intensity was measured in 2015. Similar measurements are published for city Pécs in southern Hungary [34]. As seen from the local measurements, the ITU-T *K* rain-zone of 42 mm/h is a reasonable estimation when designing radio links in Hungary.

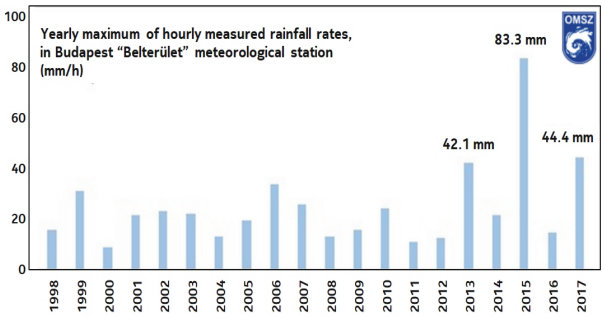

Figure 9: Yearly peak rainfall rates (mm/h) inside the territory of Budapest [33]

Long-term and high-resolution statistics of local rain events are very important to validate the ITU-R recommendations that are used in the link calculations. Beside OMSZ, BME, the Budapest University of Technology and Economics has also a meteorological station to collect long term meteorological data (rainfall rate, temperature, fog, etc.) with high-resolution [30], [35].

4.5 FDD links and the E-band frequency raster

E-band has been introduced for fixed radio communications by CEPT, the European Conference of Postal and Telecommunications Administrations [36]. Without completeness, the frequency raster is shown in Fig. 8 (750 MHz channels are not indicated). The Frequency Division Duplex (FDD) spacing between the high (H) and the low (L) frequencies is:

$$\Delta f = f_H - f_L = 10\,\text{GHz}. \tag{15}$$

Δ*f* is the 'go-return' frequency separation between the transmit and receive directions. The center frequencies are shown in Fig. 8 for the 125, 250, 500 MHz, 1 and 2 GHz bandwidth options. As seen in Fig. 8, the frequency of the low band-edge is 71 125 MHz. The Fresnel-ellipsoid has the largest diameter at this frequency. The frequency of the high band-edge is 85 625 MHz. The parabolic antennas have higher gain here, but *FSL* is also higher (Eq. 7). There are four 1 GHz wide radio bands in the raster, marked as T1/T'1, T2/T'2, T3/T'3 and T4/T'4.

5 Calculation results

Calculations have been carried out using the described method. The results are summarized in two set of plots. Antenna pairs are varying in the plots starting with ø 12- 12 cm (lowest gain) to ø 66-66 cm (highest gain). The first plot is given for a fixed hop length of a 1.2 km link. In the second set of plots, the hop length is a free variable and link availability curves are plotted for the different modulation modes from BPSK ¼ to 256-QAM.

5.1 Throughput for 1.2 km long E-band link

The estimated throughput of the 1.2 km link is calculated as a function of time. Figure 10 shows the portion of the year when fade margin is sufficient to run the link with highest modulation mode of 256-QAM. The time is marked as % of the year on the *x*-axis. In case of intensive rain, the link adaptively changes to a lower modulation mode. Parameter of the curves is the antenna pair. If both ends use ø 12 cm integrated antenna, the link cannot reach 5 Gbps and sensitive to rain. In *K* rain-zone, $R_{0.01\%}$ = 42 mm/h or stronger rainfall rate is considered in 0.01 % of the year, this is shown as 99.99 % on the horizontal axis. It is seen in Fig. 10, that ø 38 - 66 cm or ø 66 - 66 cm antenna pairs are suitable to reach 6 Gbps throughput in 99.99 % of the time.

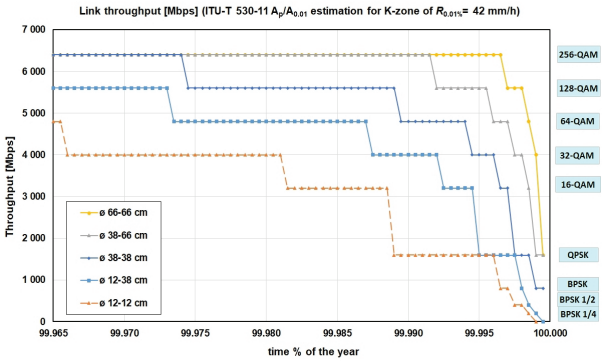

Figure 10: Estimated link throughput as a function of time (in % of the year)

It is seen, that with ø 12 cm integrated antenna pairs, the link cannot reach 6 Gbps throughput. The highest modulation mode with this antenna pair is 64-QAM in sunny days. With ø 12 - 38 cm antenna pair the modulation mode can reach 128-QAM. A peak 5 Gbps link throughput can be achieved in 99.97 % of the time. But even small rain intensities reduce the capacity of the link. Table 3 summarizes main time % figures in Available (A) and Unavailable (U) minutes. Recommended design targets are around the grey shadowed rows.

Table 3: Availability and unavailability parameters and their values in minutes in a year.

time of the year, A [%]	time of the year, U [%]	A [minutes]	U [minutes]
99.999 %	0.001 %	525 594.7	5.3
99.995 %	0.005 %	525 573.7	26.3
99.99 %	0.01 %	525 547.4	52.6
99.98 %	0.02 %	525 494.9	105.1
99.965 %	0.035 %	525 416.0	184.0

5.2 Link availabilities in the K rain-zone

In this part the calculation results are shown for estimated *E*-band link availabilities as a function of link length. Curves of Figure 11, 12 and 13 help the design considerations when new links are planned. Naturally, calculations are usually confirmed in a link planning tool. Professional planning tools help in proper channel selection, to minimize interference from neighboring links [19], [37]. Tools also support high/low coordination to avoid near-field interference. As a general design rule, high/low conflict is to be avoided. If by

mistake, different sub-band radios are planned on the same site, the planning tool provides "high/low conflict" warning.

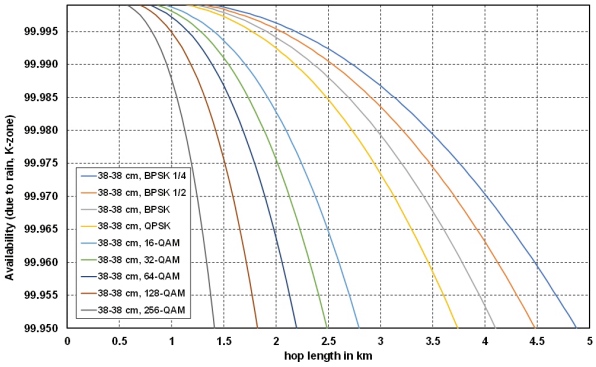

Figure 11: Link Availability as a function of hop length with ø 38 cm – ø 38 cm dish pair. The parameter is the modulation mode from BPSK ¼ to 256-QAM

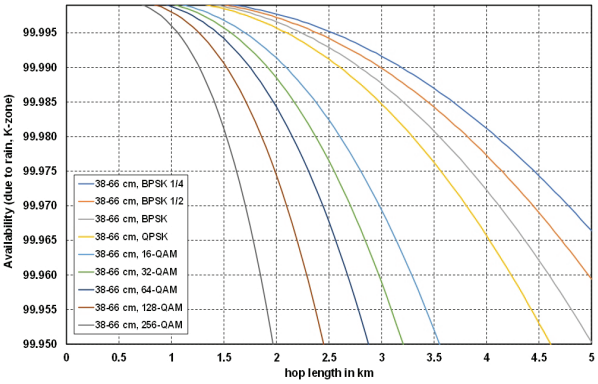

Figure 12: Link Availability as a function of hop length with ø 38 cm – ø 66 cm dish pair. The parameter is the modulation mode from BPSK ¼ to 256-QAM

6 Discussion

After reviewing the main μW/mmW link design steps, set of plots have been calculated numerically. It was shown that modulation mode dependent Fade Margin calculation is straightforward if a radio family is selected with known radio and antenna parameters. On the other hand, to calculate the effect of rain on link availability is difficult. Instead of tedious mathematical solution, a program was used to draw the plots given in part 5. Using the presented method, radio-link under-dimensioning can be avoided.

'Under dimensioned' links have small antennas for the given hop length. Even in sunny days, these links cannot reach the highest radio throughput, as adaptive modulation will not allow to reside on the corresponding modulation mode. In rainy days, under-dimensioned links reduce their symbol rate and the link throughput is quickly degrading [21]-[22]. It is worth mentioning, that for several radios, the throughput is a software licensed item [38]. There is no need to purchase a capacity what a radio link can never benefit in most of the time.

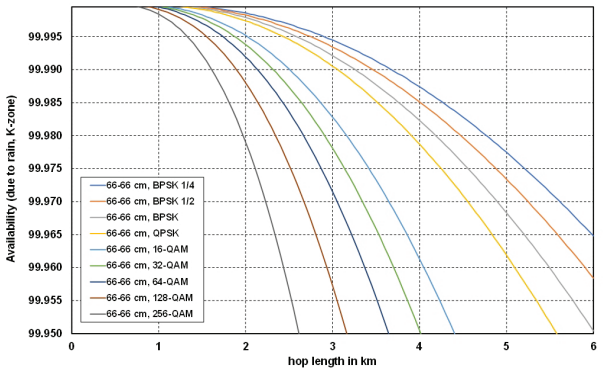

Figure 13: Link Availability as a function of hop length with ø66 cm - ø66 cm dish pair. The parameter is the modulation mode from BPSK ¼ to 256-QAM

On the contrary, 'over dimensioned' links may have too big antenna for the relative short radio hop. Unnecessarily big antennas have unpreferred visual impact on a site. Beside the undesired view, there is a dangerous mechanical problem. In wind-stormy days, strong wind may result vibration or rotation of the dishes if antenna construction is not enforced. The bigger the dish diameter, the stronger pole and antenna construction are required. At 80 GHz the antenna beamwidth is very narrow. The radiated power is focused into a sharp 'pencil' beam [17], [18]. One or even half degree of dish rotation may reduce the antenna gain easily by 3 dB [23], [24]. As presented in the calculation examples, for short hops reaching a nearby fiber access point, mainly ø 12 cm, 38 cm or 66 cm dishes are preferred.

7 Conclusions

E-band radios are excellent extensions of fiber-optical access networks. It was shown in the paper, that thanks to the wide radio bandwidth available by the frequency allocation plan [36], Gbps throughput can be achieved by state-of-the-art mmW radios. Main factor deteriorating the link availability is rain fading. The investigation focused on Central European countries like Slovenia and Hungary, where the *K* rain-zone of ITU-R with 42 mm/h rainfall rate is a good estimation in 0.01 % of the time. It was shown that with proper link design 99.99 % link availabilities or better can be achieved. Practical charts have been plotted to support the design phase of such links. As reviewed in the paper, the optical fiber is get-

ting closer and closer to the end-users in combined fiber/wireless systems (FTTH, FTTO, FTTS, 5G) [1]-[5], [7]-[8], [10]-[16], [39]-[41]. Therefore, the expected lifetime of the discussed *E*-band radio-links is 3-5 years. The investment however is not lost when optical fiber reaches a radio node. The same radio link can be quickly re-used to provide bandwidth for another hop, which is still waiting for the fiber connection.

8 Acknowledgments

The author thanks Dr. Gábor Járó and László Cserháti, (Nokia) for the useful discussions. Tamás Ludányi's (Vodafone) great experience and contribution is greatly acknowledged. The valuable support of Henrik Kiss and Brian Eichenser (CommScope) is appreciated. The author used ComSearch IQ-Link planning tool in several rollout and mobile network modernization projects.

9 Conflict of interest

The author declares no conflict of interest. This research received no external funding.

10 References

1. M. A. Ilgaz, B. Batagelj, "Določanje pomena in kakovosti radijskega dostopovnega omrežja s centraliziranim optoelektronskim oscilatorjem / Determining the importance and quality of a radio access network with a centralized optoelectronic oscillator," (in Slovenian) *Elektrotehniski Vestnik*, vol. 88, no. 4, pp. 183-189, 2021.
2. M. A. Ilgaz, "Opto-Electronic Oscillator in Radio Access Network / Optoelektronski oscilator v radijskem dostopovnem omrežju," *doctoral dissertation,* University of Ljubljana, Slovenia, 2020. [Online]. Available: https://repozitorij.uni-lj. si/IzpisGradiva.php?id=132776. [Accessed: 09-Dec-2021].
3. T. Cseh, "Improvements in Radio over Multimode Fiber Systems by Mode Filtering Techniques," *doctoral dissertation,* Budapest University of Technology and Economics, Hungary, 2018. http://hdl.handle.net/10890/5652
4. A. Hilt, E. Udvary, G. Járó, T. Berceli, "Harmonic Components and Dispersion of Mobile Network Signals due to Fiber-Optical Transmission," in *21st Optical Network Design and Modelling Conference Proceedings*, Budapest, Hungary, 2017, pp. 1-7, https://doi.org/10.23919/ONDM.2017.7958543.
5. M. A. Ilgaz, B. Batagelj, "Proposal for Distribution of a Low-Phase-Noise Oscillator Signal in Forthcoming Fifth-Generation Mobile Network by Radio-Over-Fibre Technology," in *58th International Symposium Electronics in Marine Conference Proceedings*, 2016, pp. 13-16, https://doi. org/10.1109/ELMAR. 2016.7731744.
6. J. Ladvánszky, "Circuit Theoretical Aspects of Optical Communication Links," in *17th International Conference on Transparent Optical Networks Conference Proceedings*, pp. 1-4, 2015, https://doi. org/10.1109/ICTON.2015.7193443.
7. B. Batagelj, L. Pavlovič, L. Naglič, S. Tomažič, "Convergence of fixed and mobile networks by radio over fibre technology," *Informacije MIDEM,* vol. 41, no. 2, pp. 144–149, 2011, http://www. midem-drustvo.si/Journal%20papers/MIDEM_41(2011)2p144.pdf.
8. T. Marozsák et al., "A new optical distribution approach for millimeter wave radio," in *IEEE MTT Topical Meeting on Microwave Photonics Conference Proceedings,* 1998, pp. 63-66, https://doi.org/10.1109/MWP.1998.745501.
9. G. Járó, "High speed optical receivers (in Hungarian: Nagysebességű optikai vevők)," *doctoral dissertation*, BME, Technical University of Budapest, Budapest, Hungary, 1999.
10. A. Hilt, "Transmission et traitement optiques des signaux dans les systèmes de télécommunications hertziens," *doctoral dissertation,* INPG, Institut National Polytechnique de Grenoble, Grenoble, France, 1999.
11. A. Hilt, T. Marozsák, G. Maury, T. Berceli, B. Cabon, A. Vilcot, "Radio-node upconversion in millimeter-wave fiber-radio distribution systems," in *12th International Conference on Microwaves & Radar Conference Proceedings*, vol. 1, pp. 176-180, 1998, https://doi.org/10.1109/MIKON.1998.737942
12. B. Batagelj, "Deployment of Fiber-to-the-Home in the Slovenian Telecommunications Market," *Fiber and Integrated Optics*, 2013, vol. 32, no. 1, pp. 1-11, https://doi.org/10.1080/01468030.2012.760686.
13. A. Hilt, L. Pozsonyi, "Application of Fiber-Optical Techniques in the Access Transmission and Backbone Transport of Mobile Networks," *Fiber and Integrated Optics*, vol. 31, pp. 277-298, 2012, https://doi.org/10.1080/01468030.2012.723797.
14. A. K. Garg, V. Janyani, B. Batagelj, N. H. Z. Abidin, M. H. A. Bakar, "Hybrid FSO/fiber optic link based reliable & energy efficient WDM optical network architecture," *Optical Fiber Technology*, vol. 61, pp. 1-10, 102422, 2021, ISSN 1068-5200, https://doi. org/10.1016/j.yofte.2020.102422.
15. L. Giorgi et al., "Subcarrier Multiplexing RF Plans for Analog Radio Over Fiber in Heterogeneous

Networks," *Journal of Lightwave Technology*, vol. 34, no. 16, pp. 3859-3866, 2016, https://doi.org/10.1109/JLT.2016.2581883.
16. J. Varga et al., "Reducing operational costs of ultra-reliable low latency services in 5G," *Infocommunications Journal*, vol. 10, no. 4, pp. 37-45, 2018, https://doi.org/10.36244/ICJ.2018.4.6.
17. P. Angueira, J. A. Romo, *Microwave Line of Sight Link Engineering*, John Wiley & Sons, USA, 2012.
18. T. Manning, *Microwave Radio Handy Reference Guide*, 1st ed., TMC Global, ISBN:9780648191568, Brisbane, Australia, 2019.
19. ComSearch, a Commscope Company, "IQ-Link, Microwave Link Design System," *User Guide,* version 10.4.0.7, 2021.
20. Nokia, "Nokia Wavence Ultra-Broadband Transceiver Millimeterwave 80," *Nokia data sheet*, 2021, [Online]. Available: https://www.nokia.com/networks/products/e-band-portfolio/ [Accessed: 12-Dec-2021]
21. A. Al-Saman, M. Mohamed, M. Cheffena, M. H. Azmi, T. A. Rahman, "Performance of Full-Duplex Wireless Back-Haul Link under Rain Effects Using E-Band 73 GHz and 83 GHz in Tropical Area," *MDPI Applied Sciences*, vol. 10, no. 17, 6138, pp. 1-9, https://doi.org/10.3390/app10176138.
22. A. Hilt, "Microwave Hop-Length and Availability Targets for the 5G Mobile Backhaul," in *42nd IEEE Telecommunications and Signal Processing Conference Proceedings*, 2019, pp. 187-190, https://doi.org/10.1109/TSP.2019.8768870.
23. Commscope, "VHLP1-80/A, 0.3 m / 1 ft ValuLine® High Performance Low Profile Antenna, single-polarized, 71.000 – 86.000 GHz," *antenna data sheet,* CommScope Inc., 2020.
24. Commscope, "VHLP2-80/B, 0.6m / 2 ft ValuLine® High Performance Antenna, single polarized, 71.000–86.000 GHz," *antenna data sheet,* CommScope Inc., 2021.
25. Rec. ITU-R P.676-12, "Attenuation by atmospheric gases and related effects," in *P Series, Radiowave Propagation*, *International Telecommunication Union,* Geneva, Switzerland, 2019.
26. V. Kvičera, M. Grabner, "Rain attenuation at 58 GHz: Prediction versus long-term trial results," *EURASIP Journal of Wireless Communications and Networking*, vol. 2007, pp. 1–7, https://doi.org/10.1155/2007/46083.
27. A. Hilt, T. Pap, "Application of 58 GHz band for GSM access networks in Hungary," in *11th Microwave Colloquium Conference Proceedings,* 2003, pp. 81–84, Budapest, Hungary, https://hdl.handle.net/10890/16318.
28. Rec. ITU-R P.838-3, "Specific attenuation model for rain for use in prediction methods," in *P Series, Radiowave Propagation*, *International Telecommunication Union,* Geneva, Switzerland, 2005.
29. Nokia, "The evolution of microwave transport - enabling 5G and beyond," *Nokia White Paper,* Espoo, Finland, 2019.
30. L. Csurgai-Horváth, I. Frigyes, J. Bitó, "Propagation and Availability on E-band Terrestrial Radio," in *6th European Conference on Antennas and Propagation Conference Proceedings*, pp. 73-75, 2012, https://doi.org/10.1109/EuCAP.2012.6206539.
31. Rec. ITU-R P.530-13, -18, "Propagation data and prediction methods required for the design of terrestrial line-of-sight systems," in *P Series, Radiowave propagation, International Telecommunication Union,* Geneva, Switzerland, 2009, 2021.
32. Rec. ITU-R P.837-1, -7, "Characteristics of precipitation for propagation modelling," in *P Series, Radiowave propagation, International Telecommunication Union,* Geneva, Switzerland, 1994, 2017.
33. M. Lakatos, L. Hoffmann, "Rendkívüli csapadékhullás Budapest belvárosában (in Hungarian) / Extraordinary Rainfall in Downtown Budapest," *OMSZ, Országos Meteorológiai Szolgálat,* 2017, [Online]. Available: https://www.met.hu/ismeret-tar/erdekessegek_tanulmanyok/index.php?id=1885. [Accessed: 09-Dec-2021].
34. M. Lakatos, L. Hoffmann, "Increasing trend in short term precipitation and higher return levels due to climate change," in *Országos Települési Csapadékvíz-gazdálkodási Konferencia* (in Hungarian), Cum Scientia pro Aquis Hungariae, 2017, pp. 8-16, ISBN 978-615-5845-21-5.
35. B. Adjei-Frimpong, L. Csurgai-Horváth, "Using Radio Wave Satellite Propagation Measurements for Rain Intensity Estimation," *Infocommunications Journal*, vol. 10, no. 3, pp. 2-8, 2018, https://doi.org/10.36244/ICJ.2018.3.1.
36. CEPT ECC Rec. (05)07, "Radio Frequency Channel Arrangements for Fixed Service Systems Operating in the Bands 71-76 GHz and 81-86 GHz," 2013. [Online]. Available: https://docdb.cept.org/download/9c4f8690-d0e1/REC0507.PDF. [Accessed: 09-Dec-2021].
37. A. Hilt, T. Pap, "Fixed MW Access Network Design Using Interference Matrices," in *11th Microwave Colloquium Conference Proceedings,* 2003, pp. 169–172, Budapest, Hungary, http://hdl.handle.net/ 10890/16608.
38. A. Hilt, G. Járó, "Licensing options for virtual network functions in telecommunications cloud environment," in *11th IEEE/IET International Symposium on Communication Systems, Networks & Digital Signal Processing Conference Proceedings*, 2018, pp. 1-6, https://doi.org/10.1109/CSNDSP.2018.8471802.

39. N. Badraoui, "Investigations on optical communication links for high data rate in 5G systems," *doctoral dissertation*, BME, Budapest University of Technology and Economics, Budapest, Hungary, 2020. http://hdl.handle.net/10890/15127.
40. J. Ratkoceri, "Capacity Increase of an Optical Access Network Using an Injection-locked Fabry-Perot Laser," *doctoral dissertation,* University of Ljubljana, Slovenia, 2019.
41. H. N. Parajuli, "Investigation of Potential 5G Modulation Formats in mm-Wave Radio Over Fiber Systems and Passive Optical Network," *doctoral dissertation*, BME, Budapest University of Technology and Economics, Budapest, Hungary, 2018. http://hdl.handle.net/10890/5661.

Arrived: 14. 12. 2021
Accepted: 28. 01. 2022